Estimation of spatial correlation of rain drop size distribution parameters and rain rates using NASA's S-band polarimetric radar and 2D video disdrometer network: Two case studies from MC3E

V.N. Bringi[1], L. Tolstoy[1], M. Thurai[1] and W. A. Petersen[2]
[1]Department of Electrical and Computer Engineering, Colorado State University, Fort Collins, Colorado
[2]NASA GSFC/Wallops Flight Facility, Virginia

1. Introduction

The spatial correlation of DSD parameters and rain rate at distances varying from <0.5 km to ~5-10 km is important in understanding their spatial variability for example, as related to down-scaling methodologies/modeling, to estimate the "point-to-area" variance when comparing gage/disdrometer data to radar retrievals, and application to non-uniform beam filling (NUBF) "corrections" for satellite-borne radar data which necessarily represent large pixel sizes (~4 km: TRMM and future GPM). It even applies to coarse-scale radar estimates, e.g., at long ranges where the radar beam becomes broad, or even grid-averaged products. While the spatial correlation of R has been studied extensively with dense gage networks, recently it has been shown that polarimetric radar data obtained at high spatial (close ranges<30 km) and high time resolution (PPI/RHI scan cycles <40s) offers a distinct advantage in estimating the spatial correlation function over fixed network of gages/disdrometers (Moreau et al. 2009).

On several occasions during the MC3E (Mid-latitude Continental Convective Cloud Experiment) campaign (Petersen and Jensen, 2012) in northern Oklahoma, NASA's S-band polarimetric radar, NPOL, performed repeated PPI and RHI scans over six 2D video disdrometer (2DVD) sites, located 20 to 30 km from the radar. The scans were repeated approximately every 40 seconds. We consider here two cases, one a rapidly evolving multi-cell rain event (with large drops) on 24 April 2011 and the second a somewhat more uniform rain event on 11 May 2011. We utilize these scans to determine the spatial correlation functions for the main drop size distribution parameters (D_0 and N_W) as well as rainfall rates (R). Also presented are the azimuthal variations from the PPI scans and vertical variations from RHI scans.

2. NPOL radar

NPOL radar is a research-grade dual-polarized S-band system. The nominal radar system parameters are shown in Table 1. The gate spacing is 0.15 km, with typically 1000 gates per beam.

Table 1. NASA NPOL Radar Specifications

Frequency	2.7-2.9 GHz
Polarization	H,V: simultaneous transmit & receive
Receiver	RVP8
Variables	Z, Z_{dr}, ϕ_{dp}, K_{dp} (also LDR*)
Pulse width	0.8-2 μs
PRF	250-2000 Hz
Duty cycle	0.0012 s
Antenna	8.5 m, prime parabolic, no radome
Gain	>44.5 dB
Pointing accuracy	0.1°
Beam Width	0.9°
Rotation rate	18°/s max

* *in special LDR mode*

Figure 1a in Bringi et al. (2013, this conference proceedings) shows the map of the campaign location. The white triangle in that figure depicts the area within which the 2DVDs were sited, and the area where the repeated PPI scans were performed, *viz.* over the azimuth range of 245-325 degrees, at an elevation angle 0.98 deg. The repeated RHI scans were performed at an azimuth

of 283.5 deg, over one of the 2DVD sites, with elevation angles ranging from 0-18 degrees.

Figure 1 shows a magnified view of the six 2DVD locations overlaid on rain accumulation map from the 11 May 2011 event. Note most of the intense accumulation occurred SE of the 2DVD network due to an initial period of convective cells.

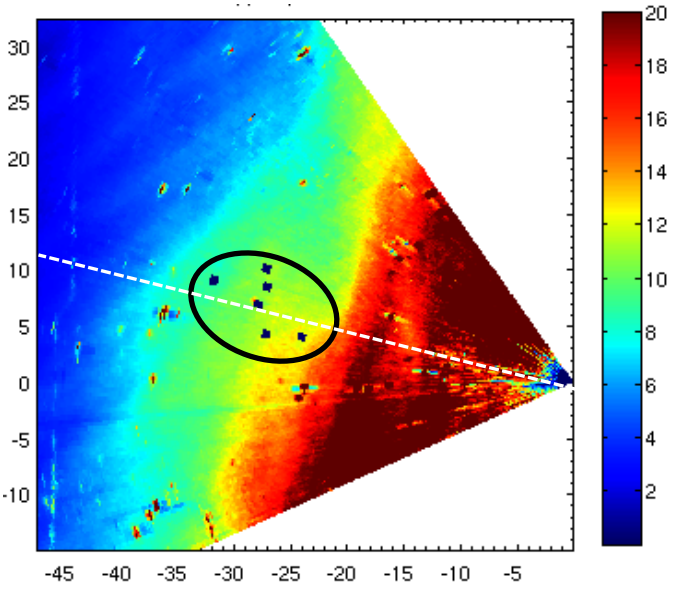

Figure 1 . Rain accumulation map from NPOL radar for May 11, 2011, 1908-2333UTC. This figure shows the PPI azimuths scan range 245-235 deg. Also shown are the approximate area where 2DVD were located, and the azimuth of the RHI scans (over SN-47 2DVD) at 283.5 deg.

3. Radar Data Processing

The separation of meteorological echoes from non-meteorological echoes was based on calculation of the standard deviation of Φ_{dp} over 10-gates moving window, with a threshold of 10° [Bringi et al 2006]. Even though the attenuation is generally negligible at S-band, the reflectivity was corrected using linear Φ_{dp} method described by Ryzhkov [2011]:

$$\Delta Z_h = 0.02\ \Delta\Phi_{dp} \qquad (1)$$

The coefficient of 0.02 is in units of dB/° and is applicable for summer-time convection in Oklahoma.

Differential reflectivity, Z_{dr} was corrected for rain attenuation as follows:

$$\Delta Z_{dr} = 0.0042\ \Delta\Phi_{dp} \qquad (2)$$

where the coefficient 0.0042 is in units of dB/°. The K_{dp} parameter was obtained using an iteratively filtered Φ_{dp} profile as described in Hubbert and Bringi (1995), and using an ad hoc "telescoping" method where variable number of gates is used, depending on the Z_h value.

Prior to calculation of rain rate, D_0, and $\log(N_w)$, the hail regions of the precipitation were filtered out, using hail signature function HDR with threshold 5 dB. Additionally, calibration offsets determined using the method described in Bringi et al. (2013, this conference proceedings) were applied for Z_h and Z_{dr}.

The 2D-video disdrometer data from 6 units were used to derive the retrieval alogrithms for D_0, N_w, R and liquid water content (LWC). The drop shapes from the 80-m fall bridge experiment from Thurai et al. (2007) and the canting angle distribution from Huang et al. (2008) were used as input to the scattering calculations.

The median volume diameter D_0 was calculated from Z_{dr} measurements as follows (D_0 in mm):

$$D_0 = 0.0536 Z_{dr}^3 - 0.1971 Z_{dr}^2 + 0.6261 Z_{dr} + 1.0815 \quad for\ Z_{dr} \geq 1\ dB$$

$$D_0 = 0.0424 Z_{dr}^4 - 0.4571 Z_{dr}^3 + 0.6215 Z_{dr}^2 + 0.457 Z_{dr} + 0.8808 \quad for\ Z_{dr} < 1\ dB \qquad (3)$$

The intercept parameter of the normalized gamma drop size distribution N_w ($mm^{-1}\ m^{-3}$) is retrieved as:

$$N_w = 19.76 \frac{Z_{h\ linear}}{D_0^{7.46}} \qquad (4)$$

The liquid water content (LWC) parameter was calculated as

$$LWC = 3.4566 * 10^{-4} \frac{Z_{h\ linear}}{D_0^{3.46}} \quad (5)$$

The rain rate was calculated using the composite algorithm (see Ryzhkov et al. 2005) from input parameters Z_h, Z_{dr}, K_{dp}:

$$R(Z_h) = 0.0229(Z_{h\ linear}^{0.6425}) \quad (6)$$

$$R(K_{dp}) = 34.3\left(K_{dp}^{0.757}\right) \quad (7)$$

$$R(Z_h, Z_{dr}) = 0.0142 \frac{(Z_{h\ linear}^{0.77})}{(Z_{dr\ linear}^{1.67})} \quad (8)$$

The block diagram illustrating the composite algorithm is given in Figure 6 of Bringi et al. (2013; these conference proceedings).

a) Correlation coefficients from RHI scans

Vertical correlation coefficients are calculated from the repeated RHI scans. Each of the three variables, i.e. N_W, D_0 and R, denoted by *v,* was interpolated from radar coordinates (elevation, distance) to the Cartesian coordinates (x,z) grid. The dimensions of each cell of the grid were chosen to be 150m x 100m, so that horizontal spacing corresponds to that of the original radar data. The RHI scans were repeated every 40 s at fixed azimuth angle (see Figure 2 which shows the time axis and volume V). The selected data begins at a height of 0.6 km from the ground (to avoid problems due to ground clutter) and ends at the bright band height of approximately 2.5 km along the vertical, and begins at 15 km range and ends at approximately 38 km range (for April 24 data) in radial direction. Then for each variable *v,* the 3-dimensional volume *V* was created in Matlab. Each volume has dimensions PxHxT, where P is the total number of cells in the radial (after gridding referred to as the horizontal) direction, H is a total number of cells of interpolation grid in vertical direction, and T is a total number of RHI scans made by radar in the time interval of interest.

The resulting matrix of Pearson's correlation coefficients **C** has dimensions PxH, each element of this matrix was calculated using Matlab function *corr()*, which compares two 1-dimensional arrays of data, each one is a time sequence (meaning it includes data at specific position *(g,h)* of all RHI scans 1..T of the time interval of interest):

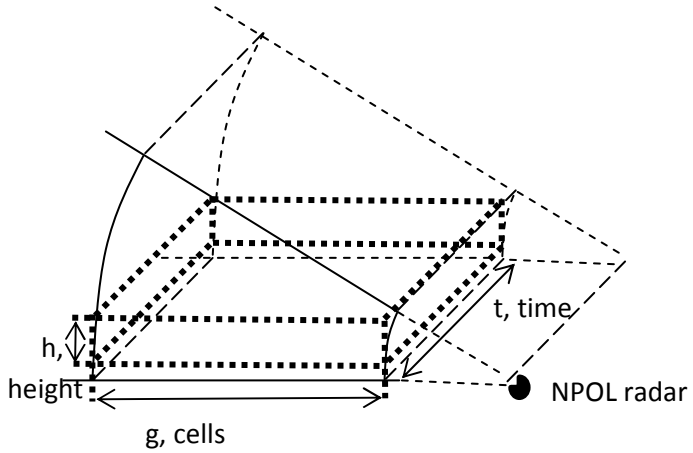

Figure 2: The 3-D volume V (dotted line) after interpolation from cylindrical (radar) coordinates into Cartesian coordinates and limiting lover altitude to 0.6 km and upper altitude to 3 km, created for each radar variable vg,b,t, and NPOL radar.

$$c_{gh} = corr(v_{g\,1\,1\_T}, v_{g\,h\,1\_T}) \quad (9)$$

where *g* is a cell number in horizontal direction, starting from the beginning mark (20 km from the NPOL for April 24 case), *h* is a cell number in vertical direction, starting from the lowest height mark (0.6km "base" or reference height). At each horizontal position, the lowest, or "base" time sequence $v_{g\,1\,1..T}$ is sequentially compared to each time sequence $v_{g\,h\,1..T}$ above it , to get a column of correlation coefficients in the matrix **C**.

To reduce "noise', the time sequences were smooth using a weighted moving average filter with window size 9 (recall RHI scans were repeated every 40 s), which corresponds to approximately 2.5 minutes. Only those elements which were not NaN in the time sequences were used. The

smoothing window selected is somewhat ad hoc and a compromise to arrive at 'reasonable' Pearson correlation coefficients along the vertical direction.

c) Correlation coefficients from PPI scans

To calculate the correlation coefficients for each variable v from the repeated PPI scans, the 3-dimensional volume *V* was created in Matlab. It has dimensions GxBxT (see Figure 3), where G is the total number of gates in the radial direction (from the start range), B is the total number of beams in a single PPI scan, and T is a total number of scans in the time interval of interest.

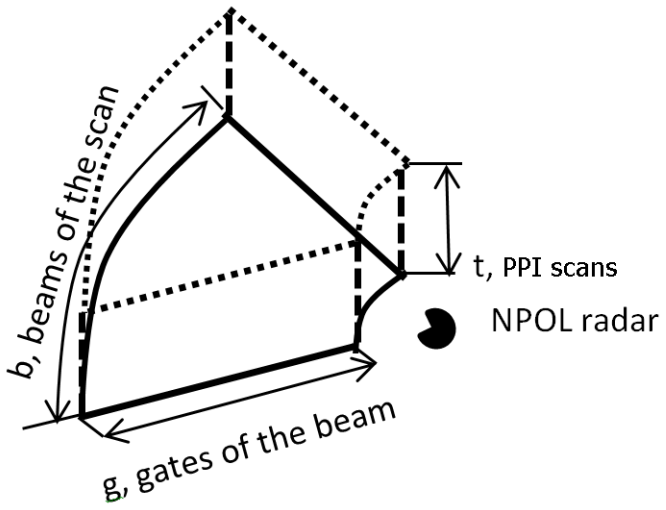

Figure 3: The 3-D volume V, created for each radar variable v, and NPOL radar.

As before, the resulting matrix of Pearson's correlation coefficients **C** has dimensions GxB, and each element of this matrix was calculated using the Matlab function *corr()*, which compares two 1-dimensional arrays of data, each one being the time sequence (meaning it includes interpolated data at specific position *(g,b)* of all PPI scans 1..T of the time interval of interest):

$$\mathbf{c}_{gb} = corr\left(v_{1\,b\,1..T}, v_{g\,b\,1..T}\right) \qquad (10)$$

where *g* [1..G] is the number of the gate from the starting point, and *b* [1..B] is the number of the beam. Here the "base" time sequence for each beam is the closest to the radar in the range of interest, and is sequentially compared to those further from the radar, thereby creating a column of correlation coefficient values in matrix C.

To eliminate any problems due to noise, each time sequence was smoothed using a moving average filter with the same parameters as for the RHI. Only those gates which were not-NaN in both "base" and "next-in-range" time sequences were compared.

4. Results and Discussion

a) NPOL scans and 2DVD data

As mentioned earlier, the repeated PPI scans on the 11th of May 2011 had covered the six 2DVD sites (see also Figure 1). Bringi et al. (2013, these conference proceedings), compared Z_h, Z_{dr} and R determined from the NPOL radar data with the simultaneous measurements from all six 2DVDs. Very good agreement was found for all three quantities, and, furthermore, rain accumulations also showed good agreement.

In Figure 4 we show the corresponding time series comparisons for D_0. For NPOL data-based estimation, eq. (2) was used to determine D0 whilst for 2DVD data based estimation, 1 minute DSDs were used for fitting to the normalized gamma distribution. Excellent agreement is found between the two time series comparisons in all six panels.

Figure 5 shows the corresponding comparisons for the 24 April 2011 event, which was a much more rapidly evolving storm. D_0 values can be seen to vary rapidly, for example, from 3 mm to less than 1 mm within 30 minutes for SN36. Even so, the agreement between the NPOL derived D_0 and the 2DVD measured D_0 are very good, except perhaps at the beginning of the storm where drop sorting may play a role.

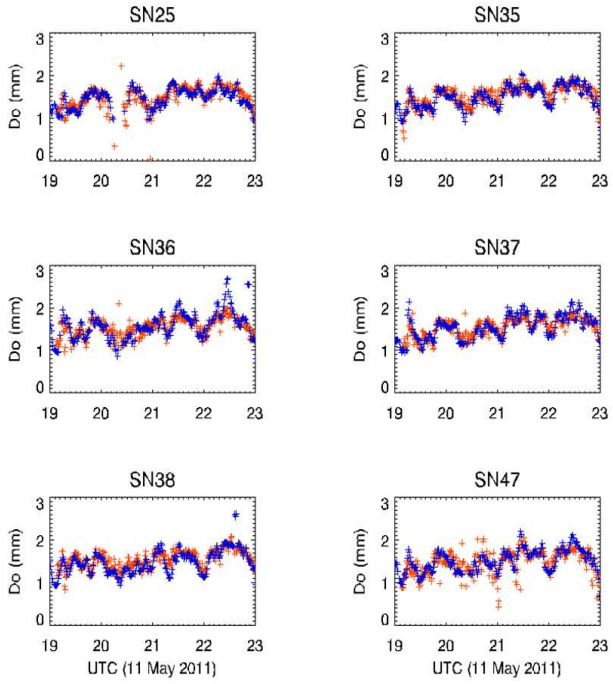

Figure 4. Time series comparison of D_0 for the 11 May 2011 event from NPOL (red line) and from 2DVD (blue line) for the six 2DVD locations (the serial numbers of the instruments are shown at the top of each panel).

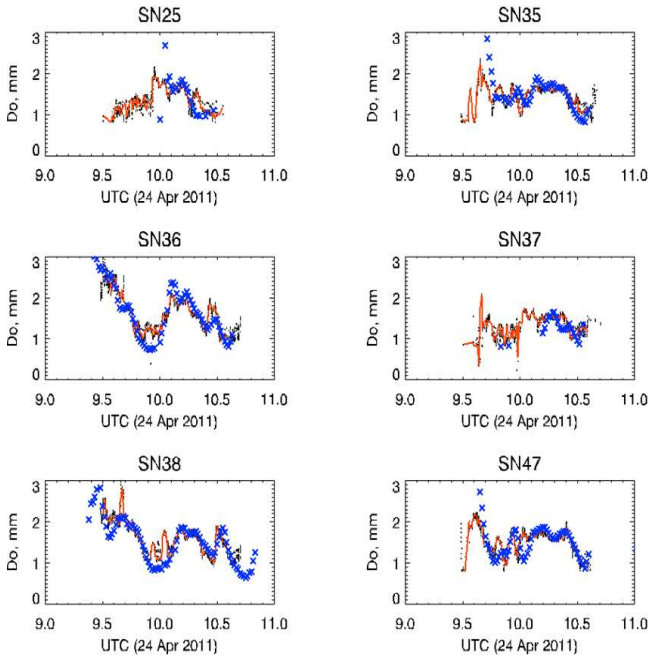

Figure 5: Time series comparison of D_0 for the 24 April 2011 event.

b) Spatial correlations from PPI scans

For each of the variables D_0, $\log_{10}(N_W)$ and R, we compute and plot a 2-D map of correlation coefficients which demonstrates the decrease of correlation coefficient as a function of range for each azimuth angle. Figure 6 shows these plots for D_0 for the two events. The decrease in the correlation coefficients is evident in both cases, but for the 24 April 2011 case, the uniformity of this decrease across the azimuth angle sector is much less compared with the more stratiform rain event on May 11, 2011.

From the set of correlation coefficients at a fixed range (starting reference range at ~16 km) through the angular sector, we construct the CDF of the spatial correlations (ρ), and compute the 10^{th}, 50^{th} (median) and 90^{th} percentile values. This is repeated at range increments of 150 m (radar gate spacing). Such an approach gives a "pseudo"-1D spatial correlation at the same time giving an estimate of its cross-beam (azimuthal) variability.

Figures 7, 8, and 9 show the pseudo-1D spatial correlation for the three variables, D_0, $\log(N_W)$, and R for the May 11 event for the 10^{th}, 50^{th} and 90^{th} percentiles. The resulting variations are compared with those derived from the 1-minute DSDs from the six 2DVDs for May 11, where each circle corresponds to one pair of 2DVD (a total 15 combinations for six 2DVDs). The same correlation algorithms were used for NPOL and 2DVD based results. The comparisons show good agreement between correlation coefficients calculated using pairs of disdrometer data and NPOL correlation coefficient statistics, especially for D_0 (Figure 7). The $\log(N_w)$ and R correlations from 2DVD fall between the 50^{th} and 90^{th} percentiles from radar. Note that the rain rate correlation falls off significantly 'faster' than either D_0 or $\log(N_W)$.

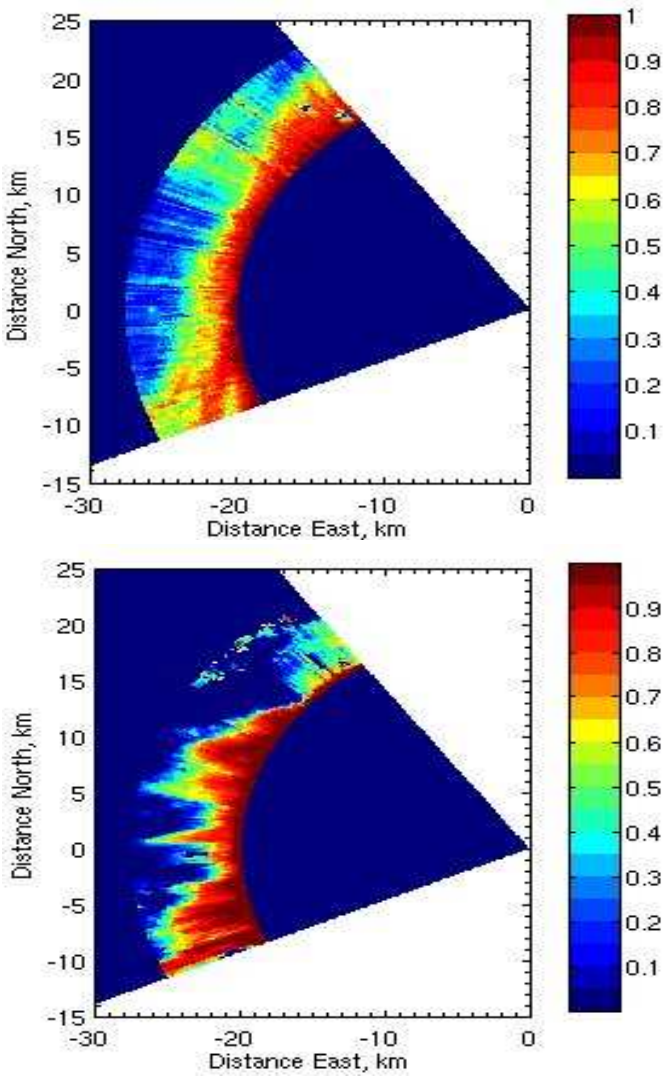

Figure 6. PPI maps of D_0 correlation coefficients for May 11 (stratiform case, top image) and April 24 (convective case, bottom image).

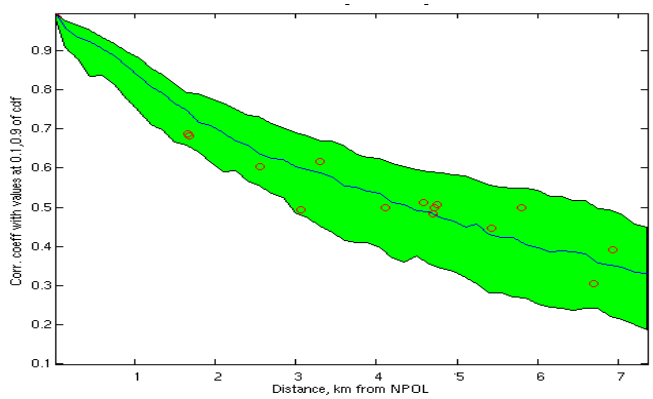

Figure 7. May 11, stratiform case. Statistical analysis of D_0, 10%, 50%, 90% percentiles of correlation coefficient, compared to correlation coefficients calculated from 2DVD data pairs.

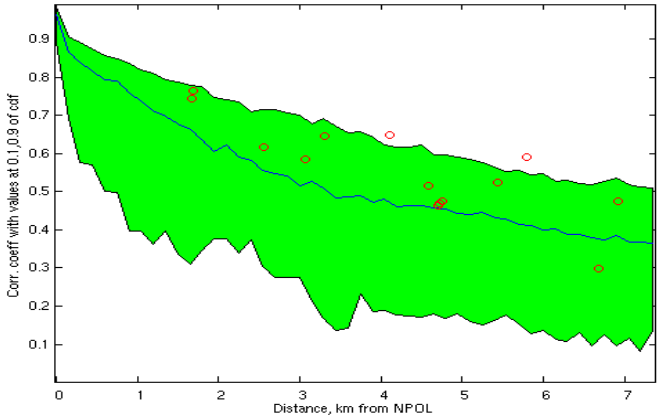

Figure 8. May 11, stratiform case. Statistical analysis of log(N_w) data, 10%, 50%, 90% percentiles of correlation coefficient, compared to correlation coefficients calculated from 2DVD data pairs.

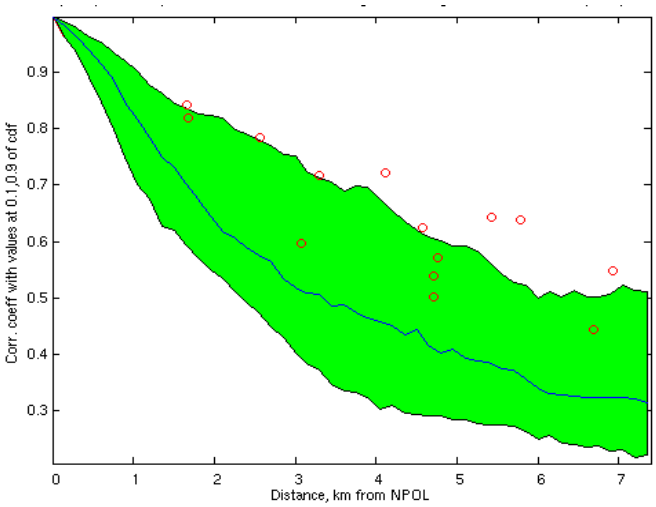

Figure 9. May 11, stratiform case. Statistical analysis of precipitation data, 10%, 50%, 90% percentiles of correlation coefficient, compared to correlation coefficients calculated from 2DVD data pairs.

Moreau et al (2009) and Bringi et al. (2011) have demonstrated that a rapidly-scanned (30-60 sec) dual-polarization (DP) radar can provide robust estimates of the rain rate spatial correlation. Here the underlying methodology relies on a three-parameter scaled exponential correlation function as used in Gebremichael and Krawjeski, (2004):

$$\rho(d) = \rho_0 \exp[- (d/R_0)^F] \qquad (7)$$

where d is the distance between measurement points, R_0 is the decorrelation (1/e) distance, F is a shape parameter and ρ_0 is the correlation when

d=0 (i.e. the "nugget" parameter). The Moreau et al. and Bringi et al. studies used (7) with DP-algorithm retrieved rainfall rates to examine error structure demonstrated the robust capability of DP-radar to estimate the 'areal' or pixel-scale correlation function. A key conclusion of these studies is that in contrast to longer duration deployments of gages, DP radar-based rain rates can be used to estimate the 'areal' correlation function at a spatial resolution of 1 km^2 or better from far fewer rain events due to the much greater areal coverage and sample numbers provided. The spatial correlation function for the DSD parameters have also been derived from a C-band DP radar by Thurai et al. (2012).

In Table 2 we show the fitted parameters:

Table 2. Fitting coefficients R_0, F for variables D_0, $\log(N_w)$, and precipitation for PPI data of stratiform case May 11.

	R_0	F
D_0	15.6397	0.75875
R	3.9072	1.1951
N_w	12.9801	0.81136

b) Vertical correlations from RHI scans.

To determine vertical correlations, we use the repeated RHI scans which were made along an azimuth of 283.5 deg as part of the scan sequence. For each variable we compute and plot a map of correlation coefficients, which demonstrates the decrease of correlation coefficient as a function of height for each range. In all cases, the reference height was set to be 0.6 km in order to avoid problems due to ground clutter. Figure 10 shows these plots for D_0 for the two events. The decrease in the correlation coefficients is evident in both cases, but for the 24 April 2011 case, the decrease is considerably faster compared with the more stratiform rain event on May 11, 2011.

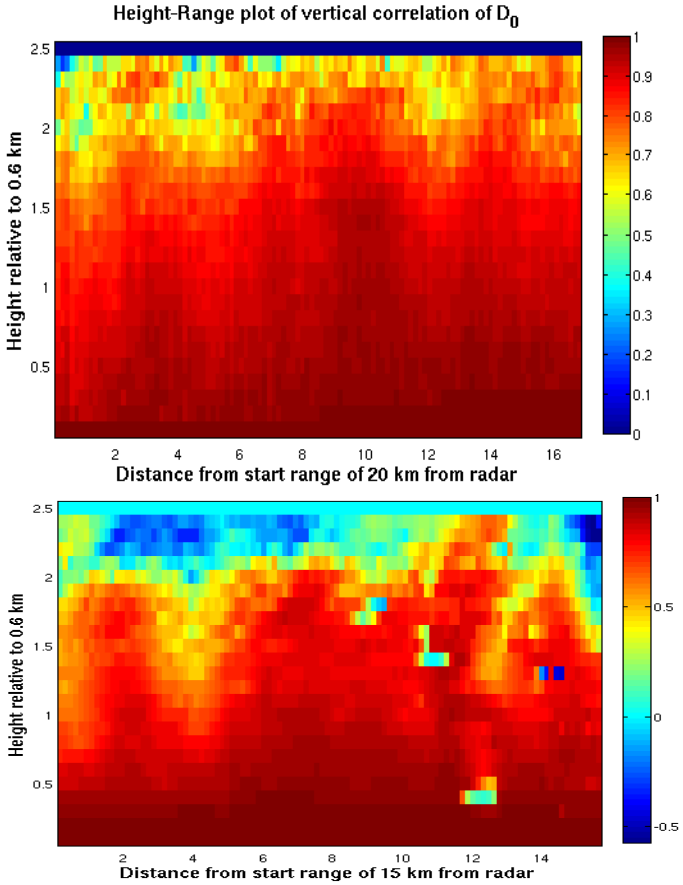

Figure 10. RHI maps of the D_0 correlation coefficients for May 11 (stratiform case, top image) and April 24 (convective case, bottom image). Vertical reference height is 0.6 km in both cases, May 11 radial reference distance is 20 km (and extends to 38 km), April 24 radial reference distance is 15 km (and extends to 33 km).

Analogous to the derivation of horizontal correlations from the PPI scans, the set of correlation coefficients at a fixed height (starting reference height at 0.6 km) and along the radial direction are used to construct the appropriate CDF of the spatial correlations (ρ), and compute the 10th, 50th (median) and 90th percentile values. This is repeated at height increments of 100 m. This will yield the "pseudo"-1D height correlation at the same time giving an estimate of along-range variability.

Figures 11, 12, and 13 show the pseudo-1D height correlation for the three variables, D_0, and $\log(N_W)$ for the May 11 and the 24 April events, for the 10^{th}, 50^{th} and 90^{th} percentiles. Note in both cases, the correlation falls off significantly 'faster' for the 24

April event which was predominantly convective rain compared with the May 11 event which had more stratiform rain. Figure 13 compares the 50th percentile curves from the two events to show more clearly the differences in the vertical correlations as a function of height between the convective and the stratiform events. Also included are the fitted curves (i.e. fitted to eq. 7, where '*d*' now represents the height relative to 0.6 km above ground level). The fitted coefficients are given in Table 3. Note once again the nugget parameter ρ_0 is 1 by definition at the reference height.

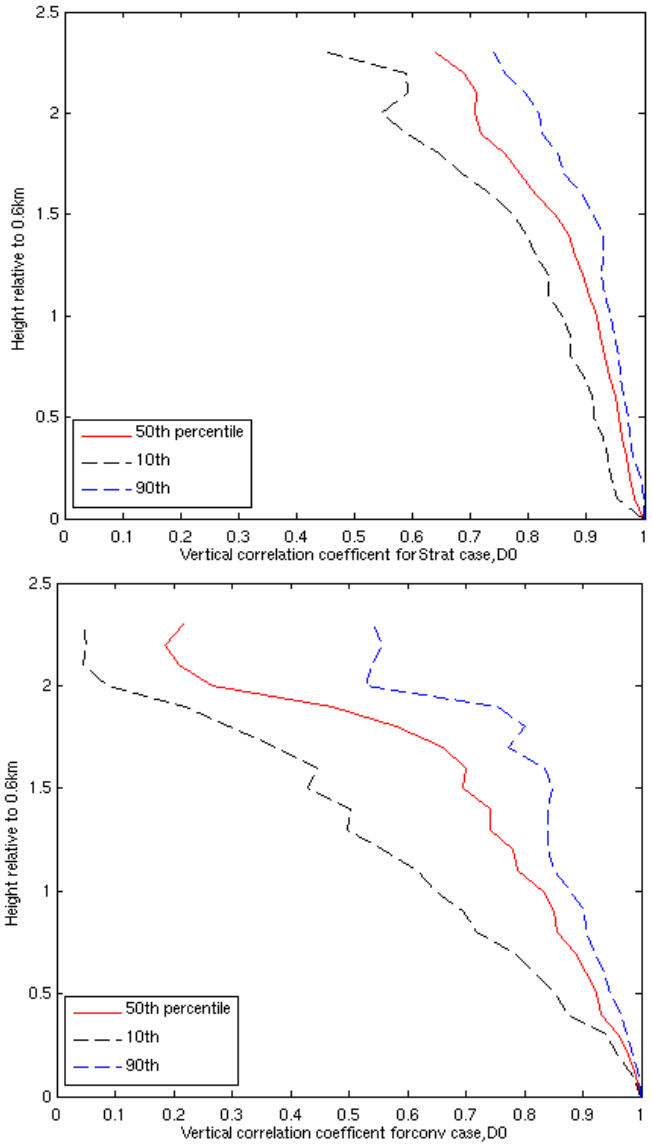

Figure 11. Comparing D_0 percentiles for May 11 stratiform case (top) and April 24 convective case (bottom).

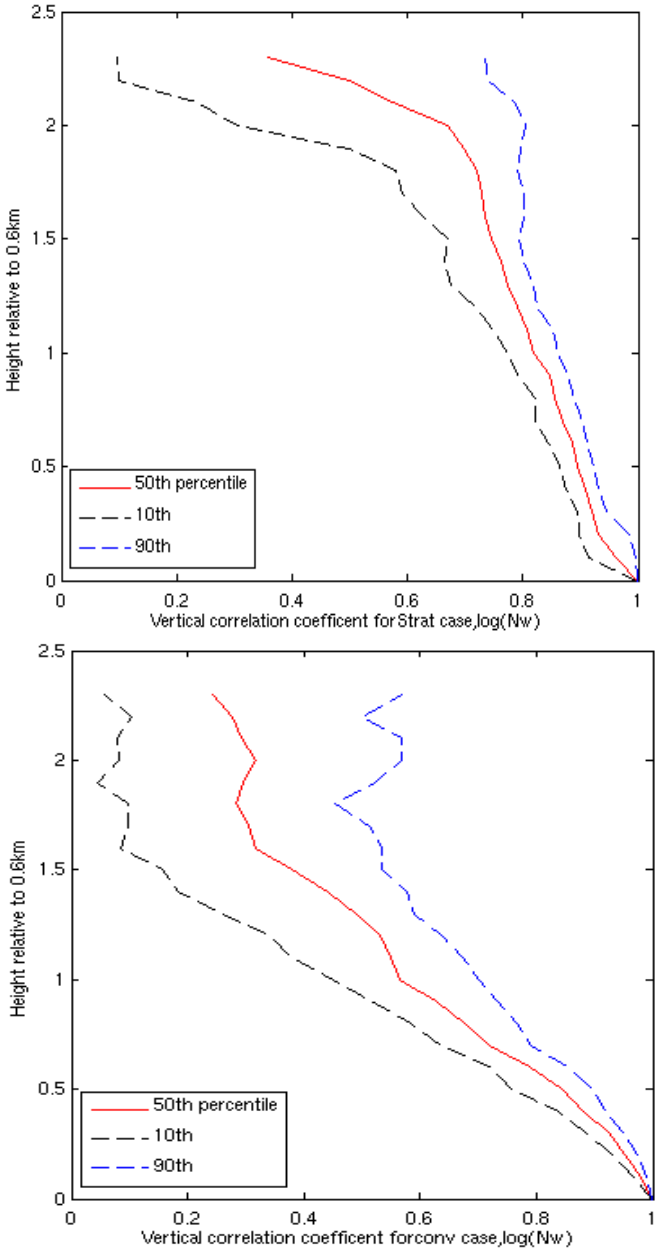

Figure 12. Comparing log(N_w) percentiles for May 11 stratiform case (top) and April 24 convective case (bottom).

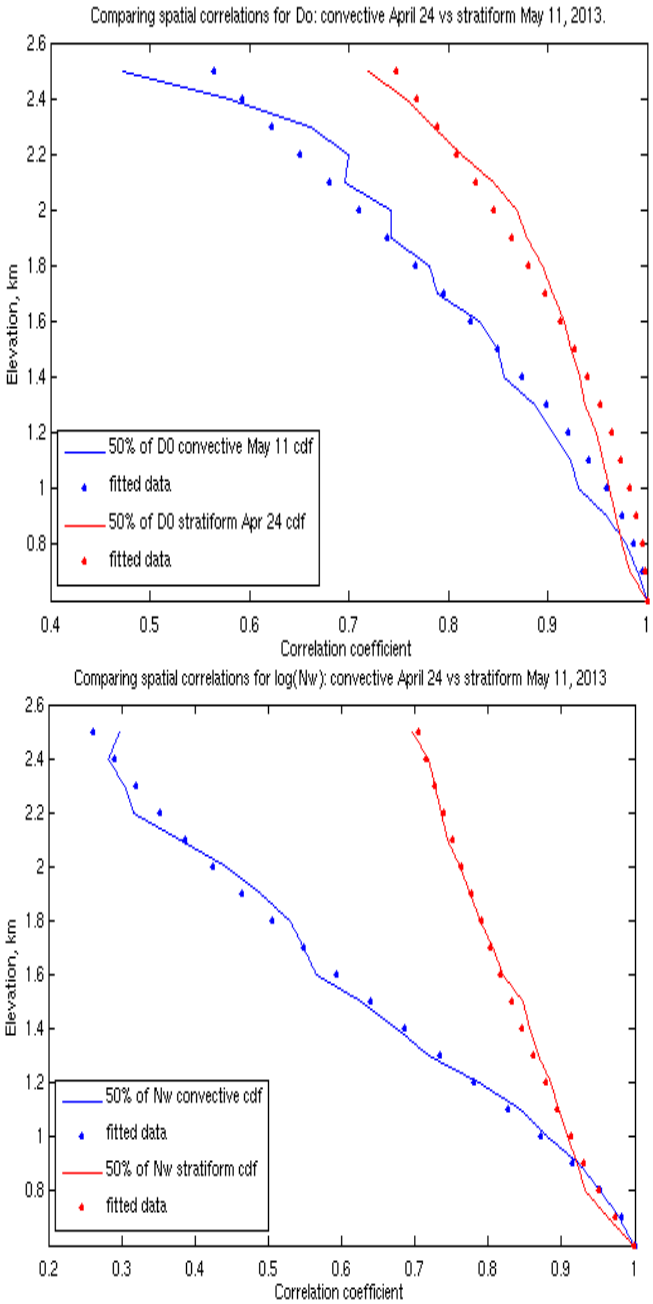

Figure 13. Comparison of correlation coefficient for RHI, for Do, log(N_w), for convective case April 24 and stratiform May 11, including fitted data (dotted plots).

Table 3. RHI, Fitting coefficients R_0, F for variables D_0, log(N_w), for RHI data of convective case April 24 and stratiform case May 11.

	R_0	F
D_0 convective	2.6477	1.6806
D_0 stratiform	3.7761	1.8003
log(N_w) convective	1.5554	1.4669
log(N_w) stratiform	6.4399	0.8604

5. Summary

Two events during the MC3E campaign have been analyzed using NPOL radar data and a network of closely-spaced six 2DVD instruments. One event (24 April 2011) was strongly convective and was of much shorter duration (< 75 min) over the 2DVD network, and the second event (11 May 2011) was of longer duration (around 4 h) and much more widespread, with large areas of stratiform rain.

Retrieval algorithms for D_0, N_W and R were derived using the 2DVD data and applied to NPOL data as a validation check. From the repeated PPI scans, with 40 second cycle time, it was possible to derive the spatial (horizontal) correlations for the two events at high space-time resolutions (typically several minutes after smoothing the time series data and at the base spatial resolution of the radar data at ranges < 30 km). Thus, the spatial correlations from radar may be described as 'areal' or 'pixel' based as opposed to 'point' spatial correlations derived from rain gages or disdrometers. The 11 May event showed considerably less azimuthal dependence than the 24 April event – as expected. Spatial correlations of D_0, N_W and R were also derived from the network of 2DVDs (using 1-minute time series, but smoothed over 3 min) and found to be in good agreement with the NPOL-based estimates. It was also noted that the rain rate correlation falls off significantly 'faster' than either D_0 or log(N_W), and that D_0 falls off the 'slowest' with respect to distance.

In an analogous manner, vertical correlations were derived from the repeated RHI scans, also with a cycle time of 40 seconds. In general, the vertical correlations fell of faster (with height) for the convective event on 24 April compared with the 11 May stratiform event.

Both the horizontal and the vertical correlations were fitted to an exponential decay function with two parameters, namely, decorrelation distance and shape factor. These fitted values should be of use in several applications such as understanding

the spatial variability of DSD parameters and rainfall rates, for example, as related to down-scaling methodologies/modeling, to estimate the "point-to-area" variance when comparing gage/disdrometer data to radar retrievals, and application to non-uniform beam filling (NUBF) "corrections" for satellite-borne radar data which necessarily represent large pixel sizes (~4 km: TRMM and future GPM). It even applies to coarse-scale radar estimates, e.g., at long ranges where the radar beam becomes broad, or even grid-averaged products. In many of the above applications the assumptions of isotropy of the spatial correlation function as well as stationarity of the underlying process needs to be invoked which have yet to be addressed.

ACKNOWLEDGEMENTS

We would like to thank the NPOL radar scientists and technicians as well as the disdrometer field technicians during MC3E for collecting the data used in this study. We would also like to thank Dr R Kakar of the NASA Precipitation Measurement Mission and Dr A Hou and Dr M Schwaller of the NASA GPM program offices for providing funding for this study.

REFERENCES

Bringi, V. N., M. Thurai, W. A. Petersen, and P. N. Gatlin, Using a network of 2D video disdrometers for external radar calibration of NASA's S-band polarimetric radar, Paper 10.3, 2013 Radar Meteorology conference, (this conference) Breckenridge, CO, September 16 - 20, 2013.

Gebremichael, M., and W. F. Krajewski, 2004: Assessment of the Statistical Characterization of Small-Scale Rainfall Variability from Radar: Analysis of TRMM Ground Validation Datasets, Journal of Applied Meteorology, 43, 1180-1199.

Huang, G-J., V. N. Bringi, V. N., and M. Thurai, 2008: Orientation angle distributions of drops after an 80-m fall using a 2D video disdrometer, J. of Atmos. and Ocean. Tech., 25, 1717-1723.

Hubbert, J. and V. N. Bringi, 1995: An Iterative Filtering Technique for the Analysis of Copolar Differential Phase and Dual-Frequency Radar Measurements, J. Atmos. Ocean Tech., 12, 643-648.

Moreau, E., J. Testud and E. Le Bouar, 2009: Rainfall spatial variability observed by X-band weather radar and its implication for the accuracy of rainfall estimates, Advances in Water Resources, 32, 1011-1019.

Petersen W., and Jensen, M., 2012: The NASA-GPM and DOE-ARM Midlatitude Continental Convective Clouds Experiment (MC3E), The Earth Observer, Volume 24, Issue 1, January - February 2012, pp. 12-18.

Ryzhkov, A. V., S. E. Giangrande, and T. J. Schuur, 2005: Rainfall Estimation with a Polarimetric Prototype of WSR-88D. Journal of Applied Meteorology, 44, 502-515.

Thurai, M., G-J. Huang, V. N. Bringi, W. L. Randeu, and M. Schönhuber, 2007: Drop Shapes, Model Comparisons, and Calculations of Polarimetric Radar Parameters in Rain, Journal of Atmospheric and Oceanic Technology, 24, 1019-1032.

Thurai, M., V. N. Bringi, L. D. Carey, P. Gatlin, E. Schultz, W. A. Petersen, 2012: Estimating the Accuracy of Polarimetric Radar–Based Retrievals of Drop-Size Distribution Parameters and Rain Rate: An Application of Error Variance Separation Using Radar-Derived Spatial Correlations. J. Hydrometeor, 13, 1066–1079.